High frequency voltage injection sensorless control technique for IPMSMs fed by three-phase four-switch inverter with a single current sensor

Journal:	*Transactions on Mechatronics*
Manuscript ID	TMECH-07-2017-6776
Manuscript Type:	Regular paper
Date Submitted by the Author:	05-Jul-2017
Complete List of Authors:	Lu, Jiadong; Northwestern Polytechnical University, School of Automation Hu, Yihua; University of Liverpool, Department of Electrical Engineering and Electronics Zhang, Xiaokang; Northwestern Polytechnical University, School of Automation Wang, Zheng; Southeast University, School of Electrical Engineering Liu, Jinglin; Northwestern Polytechnical University, School of Automation Gan, Chun; The University of Tennessee, Department of Electrical Engineering and Computer Science
Keywords:	AC motor drives, Permanent magnet motors, Fault tolerance, Synchronous motor drives
Are any of authors IEEE Member?:	Yes
Are any of authors ASME Member?:	No

High Frequency Voltage Injection Sensorless Control Technique for IPMSMs Fed by Three-Phase Four-Switch Inverter with A Single Current Sensor

Jiadong Lu, Yihua Hu, *Senior Member, IEEE*, Xiaokang Zhang, Zheng Wang, *Senior Member, IEEE*, Jinglin Liu, *Member, IEEE*, Chun Gan, *Member, IEEE*

***Abstract*—This paper proposes a sensorless control strategy using sine-wave high-frequency (HF) voltage injection for three-phase four-switch (TPFS) inverter fed interior permanent magnet synchronous motors (IPMSMs) with a single current sensor. Three phase currents are reconstructed by the single current sensor with a small modification of the inverter topology. The principle of the phase current reconstruction strategy in TPFS inverter is analyzed and the topology of the proposed drive system is illustrated. Then, the normal areas and dead zones for current reconstruction are investigated in details, and the vector synthesis method is also explained. Furthermore, the zero vector synthesis strategy and PWM generation method are also presented, where two current sampling points are applied in each PWM cycle for phase current reconstruction. Finally, HF voltage injection sensorless control strategy in the proposed drive system is realized by voltage projection on the proposed *k-l* axis coordinate system. The reconstructed phase currents track the actual ones accurately, and the estimation error of the rotor position by using the reconstructed phase currents is within ±0.1 rad. The effectiveness of the proposed scheme is verified by simulation and experimental results on a 5 kW IPMSM motor prototype.**

***Index Terms*—Fault-tolerant control, high frequency voltage injection, interior permanent magnet synchronous motor (IPMSM), phase current reconstruction, sensorless control, three-phase four-switch inverter**

I. Introduction

With the development of modern industry, the demands for reliability and cost-efficiency in the power train system increase [1]-[3]. To meet the demands, the so called fault-tolerant control technologies or money-saving solutions have been put forward. Concerning interior permanent magnet synchronous motor (IPMSM) drive system, particularly for those near the end of their operational life span periods, power switches, position sensor, and current sensor faults together with the corresponding driver or signal processing circuit faults are the commonly encountered failures as shown in Fig.1. To solve these problems, scholars proposed many solutions, namely, three-phase four-switch (TPFS) topological inverter [2]-[16], position sensorless control strategy [12], [17]-[28],

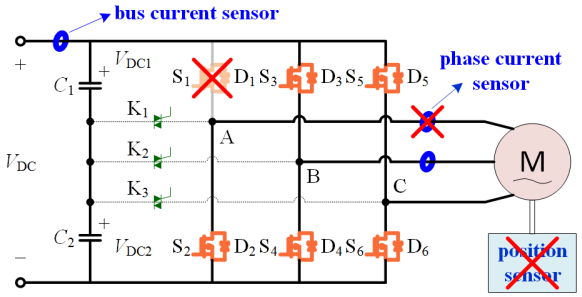

Fig. 1. Commonly occurred faults in IPMSM drive system.

and phase current reconstruction method [29]-[39]. Over the decades, these fault-tolerant control schemes have been demonstrated to have excellent performance. However, these technologies usually focus on only one specified type of hardware fault, whereas, sometimes the drive system may simultaneously face different kinds of fails. Simple combinations of the different fault-tolerant schemes are not effective, because these methods are based on the availability of other hardware components, which are obviously broken and unusable as well under this condition.

TPFS inverter is a promising topology either for fault-tolerant control solutions or money-saving purposes [3]-[7]. However, it still has some innate disadvantages compared to conventional TPSS inverters. In order to take full advantage of the considerable merits of TPFS inverter, many literatures have investigated approaches to mitigating the negative effects of TPFS topology based circuits. Papers [4] and [7] proposed control strategies to solve the problem of low voltage utilization factor. Some compensation measures were put forward in [3] and [11] to suppress voltage offset of capacitor neutral point. Paper [2] was reported to solve the problem of unbalanced currents.

Considering the sensorless control technology for IPMSMs, there are mainly two kinds of schemes: the model based methods for high speed applications and the salient pole tracking based methods for stand-still and low speed conditions. Among which, the latter is studied in this paper. High frequency (HF) signal injection is a typical strategy by using the salient pole tracking theory [18], [20]. Generally three-phase six-switch (TPSS) inverter is utilized in these

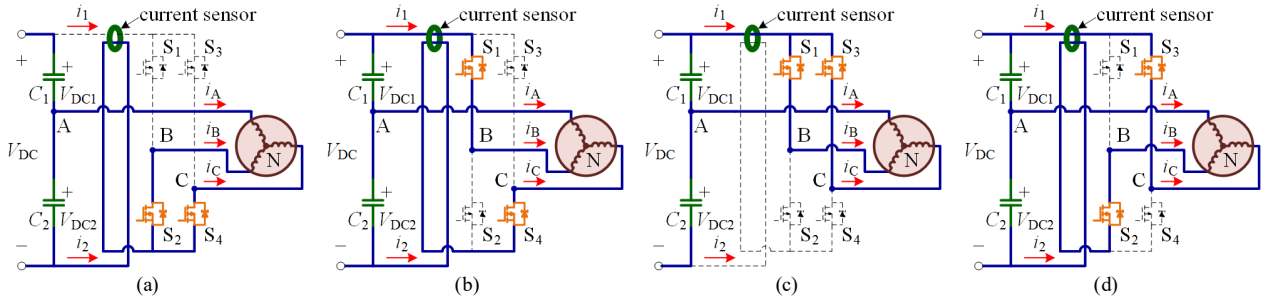

Fig. 2. The equivalent circuits of proposed IPMSM sensorless drive system fed by TPFS inverter with one single current sensor: (a) Switching state of V_{00}, (b) Switching state of V_{10}, (c) Switching state of V_{11}, (d) Switching state of V_{01}.

TABLE I
RELATIONSHIP BETWEEN THREE PHASE CURRENTS AND DETECTED CURRENT UNDER DIFFERENT SWITCHING STATES.

(S_b, S_c)	Action Vector	i_1	i_2	$i_1 - i_2$
(0, 0)	V_{00}	0	$-i_A$	$i_A = -(i_B + i_C)$
(1, 0)	V_{10}	i_B	i_C	$i_B - i_C$
(1, 1)	V_{11}	$-i_A$	0	$-i_A = i_B + i_C$
(0, 1)	V_{01}	i_C	i_B	$i_C - i_B$

schemes for signal injection and rotor position estimation [18], [20]. However, if switches in one bridge arm of TPSS inverter is broken, as have been briefly mentioned, these methods will become invalid to use due to topology change [17]. IPMSM sensorless control schemes fed by TPFS inverter was studied in [25], [26], whereas, these literatures focused on the model based methods, which are not suitable for stand-still and low speed applications. Besides, the phase currents utilized in these methods are detected by phase current sensors directly, which brings more cost increase.

Due to the limitation of current source output bandwidth, in most HF signal injection methods, the injected signal is HF rotating circular voltage rather than current signals. Because the rotor position is contained in HF components of the phase currents, precise detection of the phase currents is a matter of significance in the sensorless control system [23]. Usually this is implemented by installing three or at least two phase current sensors. Considering reliability and cost-efficiency, phase current reconstruction strategies have been proposed to remove the phase current sensors, and only one single bus current sensor is used. These methods are based on the relationship between bus current and three phase currents under different switching states [29], [38]. In order to apply the phase current reconstruction technology, vector synthesis strategy and PWM generation method need modification due to existence of the current reconstruction dead zones, which is caused by power switches dead time, diode recovery time, and AD sampling time, etc.

In this paper, IPMSM sensorless control strategy fed by TPFS inverter using a single current sensor is proposed to further increase the fault-tolerant capability of the drive system, especially when the system is near the end of its operational life span period. The proposed strategy is realized by small modification of the inverter topology and voltage projection on the proposed *k-l* axis coordinate system. The proposed strategy needs only one single current sensor and no position sensor. The principle and topology of the proposed phase current reconstruction strategy is illustrated. Afterwards, the current reconstruction dead zones and vector synthesis method are studied detailedly. Meanwhile, the zero vector synthesis scheme and PWM signals generation method are also illustrated. Finally, HF voltage injection method in the proposed drive system is deduced in detail.

This paper is organized as follows. In section II, the principle and topology of the proposed drive system are illustrated. In section III, the current reconstruction dead zones and vector synthesis method are explained. In section IV, zero vector synthesis strategy and PWM generation method are presented. In section V, HF voltage injection method in the proposed drive system is derived. Simulation and experimental results are given in section VI and VII. The conclusion is displayed in the final section.

II. PROPOSED PHASE CURRENT RECONSTRUCTION SCHEME IN TPFS INVERTER

The topology of the proposed IPMSM sensorless drive system fed by TPFS inverter with a single current sensor is illustrated in Fig.2. In the figure, the currents flow in the defined positive directions. The current sensor is installed to detect subtraction of current i_1 and i_2, i.e., $i_1 - i_2$.

In this paper, S_b and S_c are defined to denote the switching states, where "1" represents closing state of the upper switches, whereas binary "0" represents closing state of the lower switches. Therefore, relationship between the three-phase currents and detected current are displayed in Table I. From the table it can be seen that the three-phase currents can be calculated by using the detected current values along with any two adjacent voltage vectors. Simultaneously, any voltage vector can be synthesized by two adjacent voltage vectors, which makes it possible for phase current reconstruction in TPFS inverter.

III. CURRENT RECONSTRUCTION DEAD ZONES AND VECTOR SYNTHESIS METHOD

As has been mentioned before, due to the existence of power switch dead time, diode recovery time, and AD sampling time, the minimum action time T_{min} of both the two vectors used in the current reconstruction scheme is required during the whole switching period T_s. However, in some regions the action time of either one or both the two vectors is shorter than T_{min}, and the

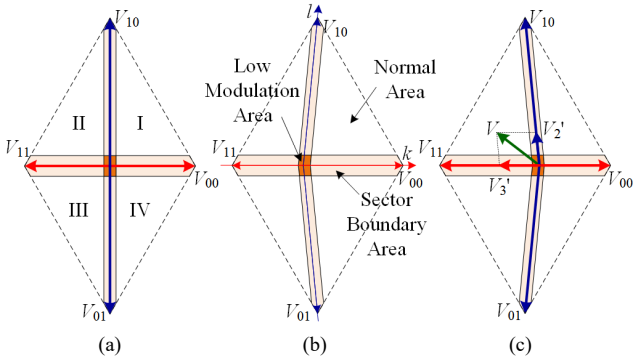

Fig. 3. Current reconstruction normal areas and dead zones in TPFS inverter: (a) $V_{DC1} = V_{DC2}$, (b) $V_{DC1} < V_{DC2}$, (c) $V_{DC1} > V_{DC2}$.

current reconstruction dead zones are formed in these regions, which are illustrated in Fig.3 (b). In Fig.3, the dead zones consist of two parts, i.e., the sector boundary area and low modulation area. In the normal areas, the vector synthesis method can be directly used for phase current reconstruction, whereas in the dead zones, the vector synthesis method have to be modulated before it can be used to reconstruct the phase currents.

In this paper, a vector synthesis method is proposed for current reconstruction. Any voltage vector is synthesized by the two basic adjacent voltage vectors. The condition $V_{DC1} < V_{DC2}$ for the two unbalanced capacitor voltages is analyzed in detail.

1) $V_{DC1} < V_{DC2}$

There are four sectors in the output voltage area as shown in Fig.4 (b). The basic vectors V_{00} and V_{11} are in the opposite directions with different values, whereas, V_{10} and V_{01} are equal in value but in the opposite directions with angular deviation. All these factors should be considered in the vector synthesis process.

In the normal areas and current reconstruction dead zones of sector I, vectors V_{00} and V_{10} are used to synthesize the output voltage both with the action time of no shorter than T_{min}, and therefore V_{11} and V_{01} are served as the compensative voltage vectors to balance the extra voltage vector. The situations in the remaining three sectors are similar. After calculation, the values in Fig.4 (b) are

$$\begin{cases} |oa| = (1-2d_{min})V_{DC2} + d_{min}(V_{DC2} - V_{DC1}) \\ |oc| = (1-2d_{min})V_{DC1} - d_{min}(V_{DC2} - V_{DC1}) \\ |ob_1| = |od_1| = (1-2d_{min} \cdot V/V_{DC1}) \cdot \sqrt{3}V/w \\ |ob_2| = |od_2| = (1-2d_{min} \cdot V/V_{DC2}) \cdot \sqrt{3}V/w \\ |oe| = \sqrt{3}V_{DC1}/2 \end{cases} \quad (1)$$

$$u = \cot\gamma = (V_{DC2} - V_{DC1}) / (2\sqrt{3}V) \quad (2)$$

$$w = \sin\gamma = 1/\sqrt{1+u^2} \quad (3)$$

where, V_{DC1} and V_{DC2} are the two bus voltage values which are illustrated in Fig.2; d_{min} is the minimum duty cycle corresponding to the minimum action time T_{min}; V represents

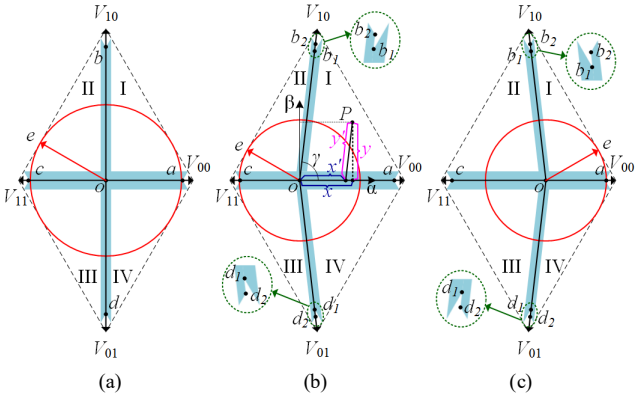

Fig. 4. Vector synthesis method in current reconstruction dead zones: (a) $V_{DC1} = V_{DC2}$, (b) $V_{DC1} < V_{DC2}$, (c) $V_{DC1} > V_{DC2}$.

the average value of the two capacitor voltages; u and w are the cotangent and sinusoidal values of γ as shown in Fig.4, which denote the fluctuation degrees of the two DC capacitor voltages.

From Fig.4 (b), it can be seen that the judgment of actual output voltage range containing the circular output voltage is based on the following condition

$$|oc| > |oe|. \quad (4)$$

By substituting (1) into (4)

$$d_{min} < \frac{2-\sqrt{3}}{4} \frac{V_{DC1}}{V}. \quad (5)$$

If the minimum duty cycle d_{min} dissatisfies (5), the actual circular output voltage will be reduced.

2) $V_{DC1} > V_{DC2}$

Similar to the above analysis, results under this condition are illustrated in Fig.4 (c), and the values in the figure are

$$\begin{cases} |oa| = (1-2d_{min})V_{DC2} - d_{min}(V_{DC1} - V_{DC2}) \\ |oc| = (1-2d_{min})V_{DC1} + d_{min}(V_{DC1} - V_{DC2}) \\ |ob_1| = |od_1| = (1-2d_{min} \cdot V/V_{DC2}) \cdot \sqrt{3}V/w \\ |ob_2| = |od_2| = (1-2d_{min} \cdot V/V_{DC1}) \cdot \sqrt{3}V/w \\ |oe| = \sqrt{3}V_{DC2}/2 \end{cases} \quad (6)$$

From Fig.4 (c), it can be seen that the judgment of actual output voltage range containing the circular output voltage is based on the following condition

$$|oa| > |oe|. \quad (7)$$

By substituting (6) into (7)

$$d_{min} < \frac{2-\sqrt{3}}{4} \frac{V_{DC2}}{V}. \quad (8)$$

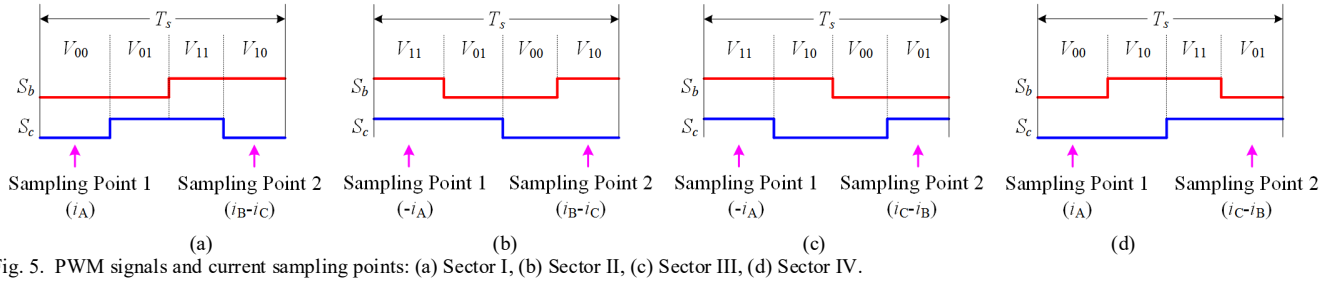

Fig. 5. PWM signals and current sampling points: (a) Sector I, (b) Sector II, (c) Sector III, (d) Sector IV.

3) $V_{DC1} = V_{DC2}$

The results derived under this condition are shown in Fig.4 (a), and the values in the figure are

$$\begin{cases} |oa| = |oc| = (1-2d_{\min})V \\ |ob| = |od| = (1-2d_{\min})\sqrt{3}V \\ |oe| = \sqrt{3}V/2 \end{cases}. \tag{9}$$

From Fig.4 (a), it can be seen that the judgment of actual output voltage range containing the circular output voltage is based on the following condition

$$|oa| > |oe|. \tag{10}$$

By substituting (9) into (10)

$$d_{\min} < \frac{2-\sqrt{3}}{4}. \tag{11}$$

With the analysis above, the voltage values under the three conditions in Fig.4 can be derived as

$$\begin{cases} |oa| = (1-2d_{\min})V_{DC2} + d_{\min}(V_{DC2} - V_{DC1}) \\ |oc| = (1-2d_{\min})V_{DC1} - d_{\min}(V_{DC2} - V_{DC1}) \\ |ob| = |od| = \left[1-2d_{\min}\cdot V/\min(V_{DC1}, V_{DC2})\right]\cdot\sqrt{3}V/w \\ |oe| = \sqrt{3}\min(V_{DC1}, V_{DC2})/2 \end{cases}. \tag{12}$$

In (12), $|ob|$ and $|od|$ represent $|ob_1|$ and $|od_1|$ respectively in both Fig.4 (b) and (c). The judgment of actual output voltage range containing the circular output voltage can be made by using the condition displayed below

$$d_{\min} < \frac{2-\sqrt{3}}{4}\frac{\min(V_{DC1}, V_{DC2})}{V}. \tag{13}$$

IV. Zero Vector Synthesis Strategy and PWM Generation Method

A. Zero vector synthesis method

TPFS inverter inherently has no zero vector, and the equivalent zero vector can only be synthesized by the four available basic vectors. In this paper all the four vectors V_{00}, V_{10}, V_{11}, and V_{01} are applied. The unequal values of V_{00} and V_{11} and the incompletely opposite directions of V_{10} and V_{01} will be taken into consideration. The action time of the four vectors can be deduced as

$$\begin{cases} T_{zero\_10} = T_{zero\_01} = t/4 \\ T_{zero\_00} = t\cdot V_{DC1}/4V \\ T_{zero\_11} = t\cdot V_{DC2}/4V \\ t = \dfrac{T_{zero}}{1 + \dfrac{|V_{DC1} - V_{DC2}|}{4\cdot\min(V_{DC1}, V_{DC2})}} \end{cases} \tag{14}$$

where, T_{zero_00}, T_{zero_10}, T_{zero_11} and T_{zero_01} are the zero vector component time of vectors V_{00}, V_{10}, V_{11}, and V_{01}, respectively; T_{zero} is the total zero vector time.

The action time of compensational vector used to balance the components of vectors V_{10} and V_{01} on the *l*-axis is

$$T_{zero\_Add} = \frac{|V_{DC1} - V_{DC2}|}{\min(V_{DC1}, V_{DC2})}\cdot\frac{t}{4} \tag{15}$$

where, T_{zero_Add} is the zero vector compensation time of vectors on the *l*-axis.

If $V_{DC1} > V_{DC2}$, the compensational vector is V_{00}, otherwise the compensational vector is V_{11}.

B. PWM signals and current sampling points

In the previous part, the zero vector synthesis method is introduced. In this paper, PWM signals are derived based on the proposed zero vector synthesis method using all the four vectors. PWM signals and current sampling points are illustrated in Fig.5. There are two bus current sampling points in each PWM cycle for phase current reconstruction.

V. Principle of HF Voltage Injection Sensorless Control Fed by TPFS Inverter

Generally TPSS inverter is utilized in IPMSM sensorless control schemes for signal injection and processing to estimate the rotor position. However, if the inverter is broken due to open-circuit fault of switches in one bridge arm, these methods will become invalid because of topology change. In order to apply the sensorless control technology in IPMSM drive system fed by TPFS inverter, some adjustments need to be made in HF voltage injection methods. HF circular voltage signal injected into the motor winding is

$$u_h = U_h e^{i\omega_h t} \tag{16}$$

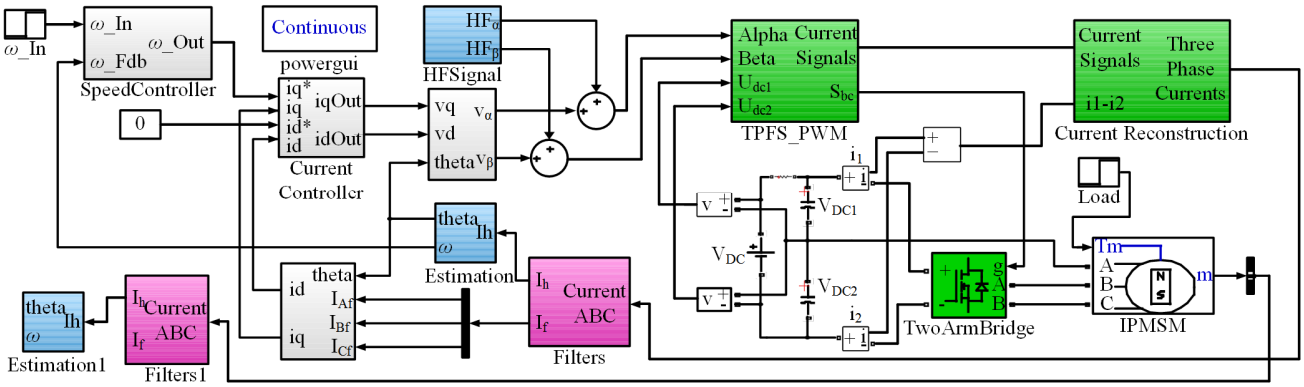

Fig. 6. PWM signals and current sampling points: (a) Sector I, (b) Sector II, (c) Sector III, (d) Sector IV.

where u_h denotes the injected HF circular voltage signal; U_h represents the amplitude of the injected signal; ω_h is the electric angular velocity of the injected signal; t represents time.

In the Clark coordinate system, the injected HF signal can be described as

$$\begin{cases} u_\alpha = U_h \cos(\omega_h t) \\ u_\beta = U_h \sin(\omega_h t) \end{cases} \tag{17}$$

where u_α and u_β represent projections of the injected HF signal on the α- and β-axis respectively in the Clark coordinate system.

In this paper, a nonorthogonal-nonlinear *k-l* axis coordinate system is utilized as shown in Fig.3 (b). In the coordinate system V_{00} and V_{11} are in the positive and negative directions of *k*-axis respectively, whereas V_{10} and V_{01} are in the positive and negative directions of *l*-axis respectively. The corresponding representation of a $P(x, y)$ on the *k-l* axis $P(x', y')$ can be deduced as (18), which is shown in Fig.4 (b)

$$\begin{cases} x' = x - u \cdot |y| \\ y' = y / w \end{cases} \tag{18}$$

where x and y are the coordinates of point P in the Clark coordinate system; x' and y' are projections of point P on the *k-l* coordinate system.

Thus the injected HF voltage signal on the *k-l* axis can be described as

$$\begin{cases} u_k = u_\alpha - u \cdot |u_\beta| = U_h \left[\cos(\omega_h t) - u \cdot |\sin(\omega_h t)| \right] \\ u_l = u_\beta / w = U_h \sin(\omega_h t) / w \end{cases} \tag{19}$$

where u_k and u_l represent projections of the injected HF signal in the *k-l* coordinate system.

Then the rotor position can be obtained by analyzing HF components of the reconstructed phase currents.

VI. Simulation Results

In order to verify the effectiveness of the proposed IPMSM sensorless control strategy fed by TPFS inverter using phase current reconstruction, simulations have been carried out in MATLAB/Simulink as shown in Fig.6. The main parameters of IPMSM used in simulation are given in Table II, and the parameters of the injected HF signal are 40V, 1000Hz. The PWM switching frequency is 10 kHz, and the minimum switching state time T_{min} is set as 5 μs. In the simulation system, phase-A winding of IPMSM is connected to the neutral point of the two bus capacitors. The reconstructed three-phase currents are utilized for position estimation and speed control. For comparison purpose, the estimated rotor position by using the actual currents are also analyzed. In addition, different working conditions of IPMSM are tested, including the starting mode, load disturbance mode, and speed reversing mode.

TABLE II
Main Parameters of IPMSM Used in Simulation and Experiment.

Parameter	Value	Parameter	Value
Rated power	5 kW	*d*-axis Inductance	4.2 mH
Inverter DC voltage	540 V	*q*-axis Inductance	10.1 mH
Rated torque	15 N·m	Phase resistance	0.18 Ω
Pole pairs	3	Maximum speed	3000 r/min
Rotor inertia	0.0023 kg·m²		

A. Phase current reconstruction strategy

Fig.7 shows the simulation results of the proposed phase current reconstruction scheme. In the figure, Sb and Sc are the PWM signals of the upper switches in phase B and C. i_1-i_2 is defined in Fig.2. i_A, i_B, and i_C represent the actual three-phase currents, respectively. i_A', i_B', and i_C' denote the reconstructed three-phase currents, respectively. 1st and 2nd are the two sampling points for current reconstruction in each PWM cycle. The 1st sampling point in each PWM cycle is marked with pink dotted line, whereas the 2nd sampling point is marked with orange dotted line.

The output voltage vector in Fig.7 is located in sector III & IV. In sector III, the 1st sampling point lies in the action period of vector V_{11}, and the value of the detected current, $i_1 - i_2$, is $-i_A$. The 2nd sampling point lies in the action period of vector V_{01}, and the value of the detected current is $i_C - i_B$. Therefore, the reconstructed three phase currents i_A', i_B', and i_C' can be calculated after the 2nd sampling point in each PWM cycle. From Fig.7 (d), it can be seen that the proposed phase current

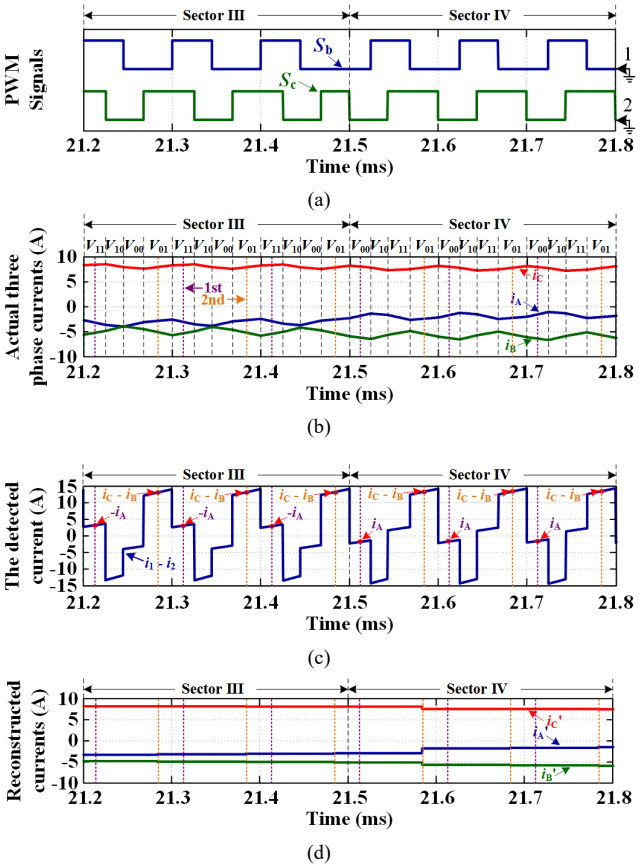

Fig. 7. Simulation results of phase current reconstruction of proposed scheme: (a) PWM signals, (b) Actual phase currents and action vector, (c) Detected current, (d) Reconstructed phase currents.

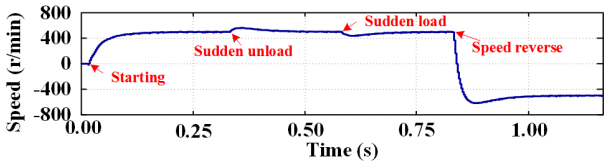

Fig. 8. Simulation results of speed response of IPMSM sensorless drive system fed by TPFS inverter.

reconstruction scheme is effective to mimic the actual three-phase currents.

B. Sensorless control performances

Fig.8 shows the speed response curve of the sensorless drive system. At 0.01 s the speed changes from 0 to 500 rpm with a load of 10 N·m. At 0.33 s a sudden load of 3 N·m is removed from the motor shaft. Then at 0.6 s a sudden load of 3 N·m is added to the motor shaft. Finally, at 0.83 s the output speed is set to -500 r/min (speed reverse).

Fig.9 shows the simulation results of the actual and reconstructed three-phase currents of the sensorless drive system. i_A, i_B, and i_C represent the actual three-phase currents, whereas i_A', i_B', and i_C' denote the reconstructed three-phase currents. From the figure, it can be seen that the reconstructed phase currents track the actual ones accurately, even in the dynamic process of the phase currents.

Fig.10 shows the simulation results of IPMSM sensorless

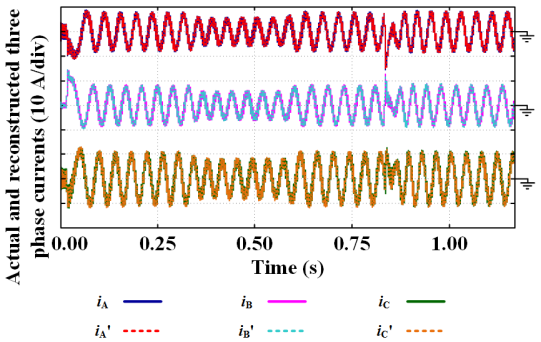

Fig. 9. Simulation results of actual and reconstructed phase currents of IPMSM sensorless drive system fed by TPFS inverter.

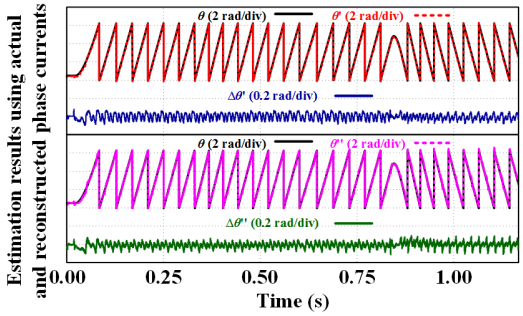

Fig. 10. Estimation results of IPMSM sensorless drive system fed by TPFS inverter using actual and reconstructed phase currents.

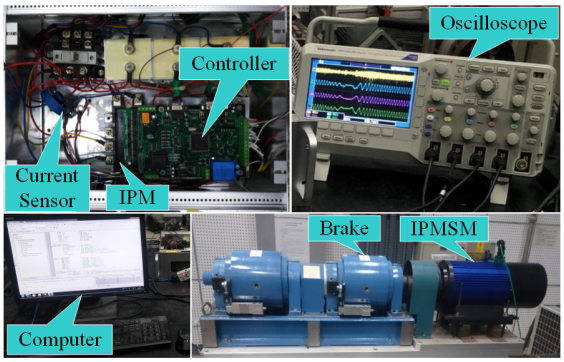

Fig. 11. Experimental setup.

control strategy fed by TPFS inverter: Fig.10 (a) shows the estimation results by using the actual three-phase currents, and Fig.10 (b) shows the estimation results by using the reconstructed three-phase currents. In the figure, θ denotes the actual rotor position. θ' and θ'' represent the estimated rotor positions using the actual and reconstructed three-phase currents respectively. $\Delta\theta'$ and $\Delta\theta''$ are the estimation errors corresponding to θ' and θ'' respectively. From the figure it can be clearly that seen that estimation errors of IPMSM sensorless drive system fed by TPFS inverter are acceptable. By applying the actual phase currents, the estimation errors are controlled within about ±0.075 rad, whereas, by applying the reconstructed phase currents, the errors are larger but are still controlled within a tolerable value of ±0.1 rad.

VII. Experimental Results

To further verify the effectiveness of the proposed IPMSM

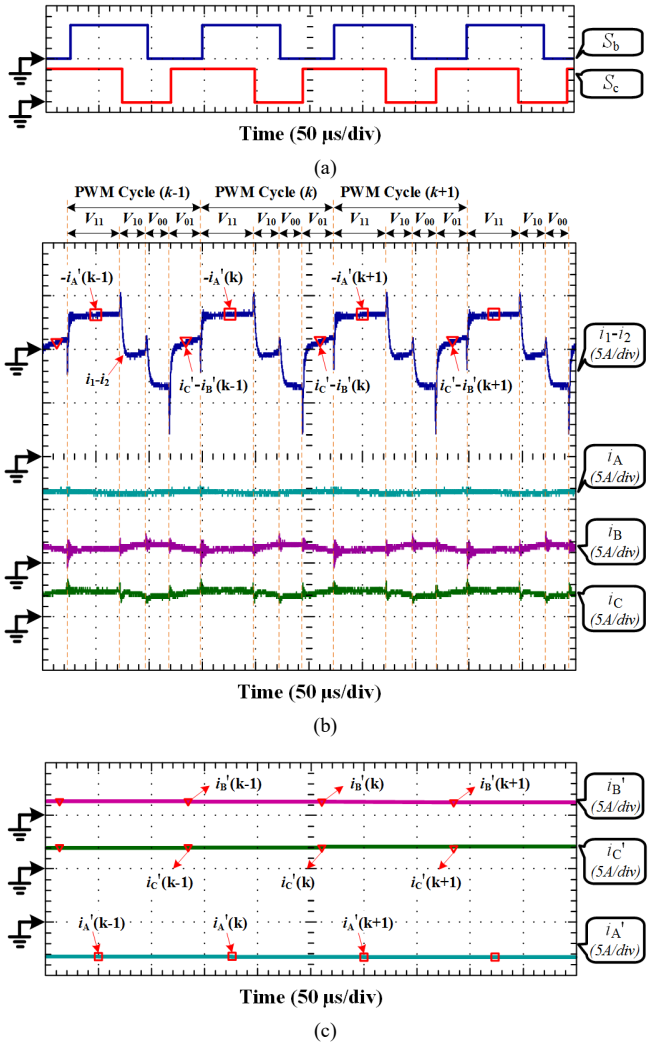

Fig. 12. Experimental results of proposed phase current reconstruction scheme (here, sector III): (a) PWM signals, (b) Detected current and actual phase currents, (c) Reconstructed phase currents.

sensorless control strategy fed by TPFS inverter using a single current sensor, an experiment platform is set up as shown in Fig.11. The main parameters of IPMSM used in experiment are displayed in Table II. The parameters of the HF signal are 30V, 1000Hz. The controller is supplied by three-phase AC voltages with the amplitude of 380 V, with a rectifier and multi-level DC output power converter installed. An intelligent power module (IPM), Mitsubishi PM75RLA120, is used as PWM-VSI with the frequency of 8 kHz. Phases B and C of the motor winding are connected to the corresponding output terminals of IPM. A single current sensor is applied in the experiment platform to detect i_1-i_2 as shown in Fig.2. On the platform, a DSP, TMS320F2812, is utilized to implement the proposed strategy, sample the current, and generate PWM signals, etc.

A. Phase current reconstruction strategy

The experimental results of the proposed phase current reconstruction scheme are displayed in Fig.12 (here, sector III). In the figure, S_b and S_c are respectively the PWM signals of the upper switches in phase B and C. i_1-i_2 is defined in Fig.2. i_A, i_B, and i_C represent the actual three-phase currents respectively. i_A', i_B', and i_C' denote the reconstructed three-phase currents respectively. Labels (k-1), (k), and (k+1) represent the PWM cycle sequences. The period of each PWM cycle is 125 μs, in which the two sampling points are in the middle of the corresponding vector periods and are marked with different symbols.

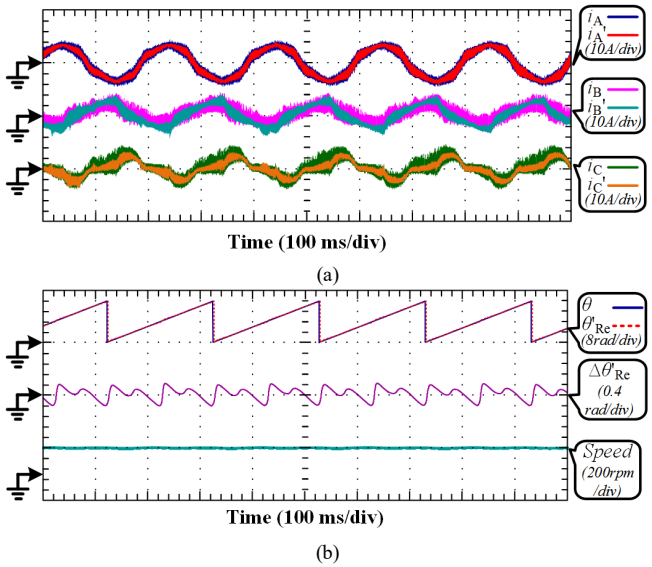

Fig. 13. Experimental results of proposed scheme in constant speed mode (speed=100 rpm): (a) Actual and reconstructed phase currents, (b) Estimation results and output speed.

In sector III, the sequences of the action vectors are V_{11}, V_{10}, V_{00} and V_{01} in each PWM cycle. Therefore, in the figure, the waveform of current i_1-i_2 has four stages corresponding to the sequences of the four vectors: $-i_A'$, i_B'-i_C', i_A' and i_C'-i_B'. The first sampling point in each PWM cycle is for current $-i_A'$ with square symbols; the second sampling point in each PWM cycle is for i_C'-i_B' with inverted triangle symbols. From the figure it can be seen that the reconstructed three-phase currents track the actual ones accurately.

B. Sensorless control performances

Fig.13 shows the experimental results of the proposed IPMSM sensorless control strategy fed by TPFS inverter using one single current sensor in the constant speed mode. Fig.13 (a) shows the actual and reconstructed three-phase currents. Fig.13 (b) presents the rotor position estimation results and the actual output speed of the drive system. The motor speed is set to 100 rpm in this condition. Compared to the actual current waveform in simulation, the experimental results have more burrs. This is due to the presence of white noise in the system and interference of the current sensor. In addition, the existence of HF current components also causes non-sinusoidal waveforms. However, the performance of the drive system is acceptable, in the figure, the estimated rotor position track the actual one accurately. The estimation error is controlled within ±0.1 rad. The output speed is stable and is controlled at 100 rpm.

To further prove the applicability of the proposed strategy, the experimental results in the starting mode are displayed in Fig.14. Fig.14 (a) illustrates the current reconstruction results. Fig.14 (b) shows the actual and estimated rotor positions

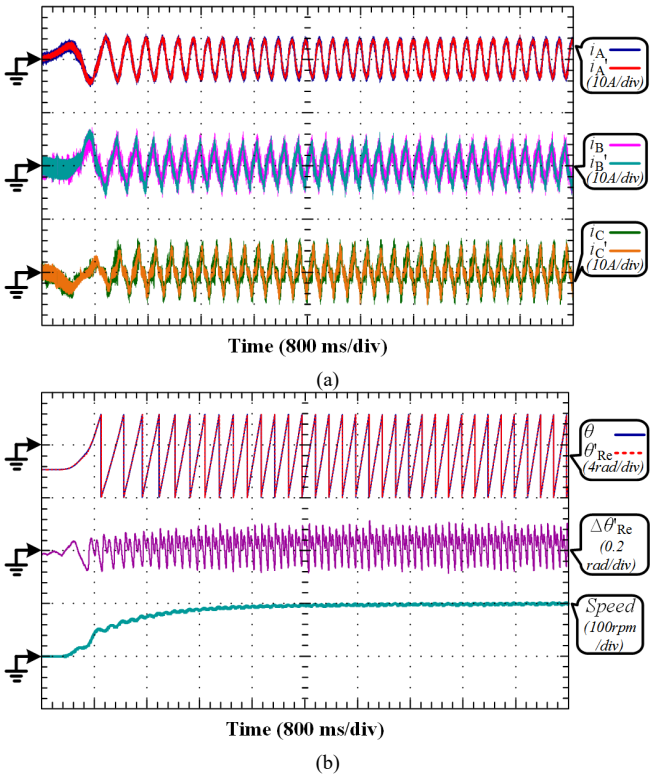

Fig. 14. Experimental results of proposed scheme in starting mode (speed from 0 rpm to 100 rpm): (a) Actual and reconstructed phase currents, (b) Estimation results and output speed.

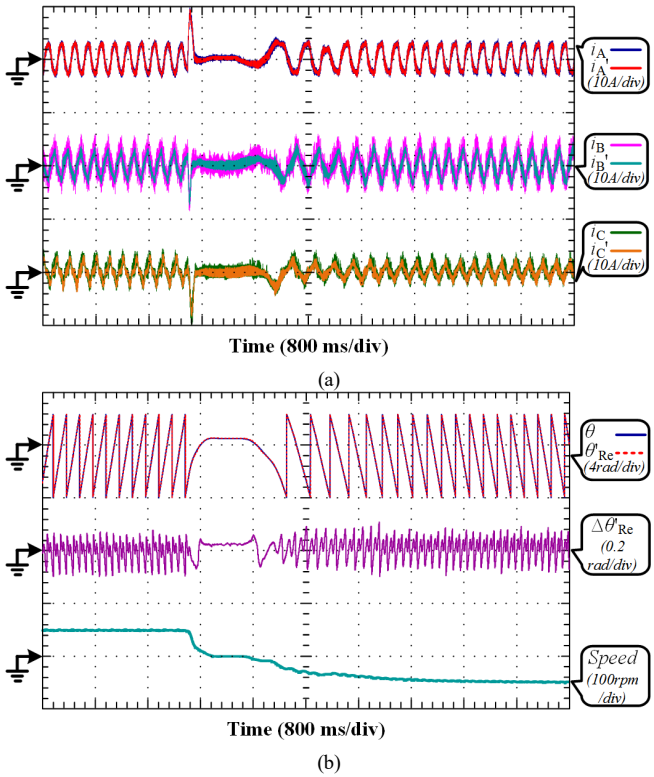

Fig. 15. Experimental results of proposed scheme in speed reversing mode (speed changes from 100 rpm to -100 rpm): (a) Actual and reconstructed phase currents, (b) Estimation results and output speed.

together with the output speed of IPMSM. In the experiment process, the motor speed command changes from 0 rpm to 100 rpm. In this case, the reconstructed three-phase currents track the actual ones well. In the figure, the estimation error is controlled within ±0.1 rad. The motor speed rises steadily from 0 to 100 rpm.

In order to validate the effectiveness of the proposed strategy in fast dynamic process of the system, experiments have been carried out in the speed reversing mode of the motor. The speed command changes to -100 rpm abruptly when the motor is running at 100 rpm steadily. The experimental results in this condition are illustrated in Fig.15. Fig.15 (a) exhibits the experimental results of the actual and reconstructed three-phase currents. Fig.15 (b) shows the experimental results of position estimation and output motor speed. In the figure, the actual currents change fast in the speed reversing process. It can be seen that in the fast dynamic process the reconstructed three-phase currents can also track the actual ones well. The estimation error is controlled within ±0.1 rad. The output motor speed follow the command smoothly from 100 rpm to -100 rpm.

VIII. Conclusion

An IPMSM sensorless control system fed by TPFS inverter using a single current sensor is proposed in this paper. To implement the proposed strategy, three-phase currents are reconstructed from the bus current by the single current sensor with minor topology change. The principle of the proposed phase current reconstruction strategy is studied in detail. The zero vector synthesis method is deduced and the corresponding PWM generation method together with current sampling points in each PWM cycle is illustrated. The sensorless control strategy using HF voltage injection in the proposed drive system is investigated. The effectiveness of the proposed IPMSM sensorless control scheme using a single current sensor is verified by the simulation and experimental results on a 5 kW IPMSM motor prototype.

The main contributions of this paper are listed as follows.

1) A low-cost IPMSM drive is proposed by using one current sensor without position sensors. The proposed TPFS inverter only needs a small modification of the inverter topology based on the conventional one, which achieves the fault-tolerant ability when one bridge arm of the inverter fails.
2) The two current sampling points for current reconstruction are within the period of action vectors in each PWM cycle. Therefore, no additional voltage pulses are required for current reconstruction.
3) A *k-l* axis coordinate system is proposed for sector identification and vector projection, which is simple and effective for the proposed strategy.

From the results, it can be seen that the reconstructed phase currents track the actual ones accurately in different working conditions, e.g., the constant speed mode, starting mode and speed reversing mode. The estimation error of the drive system by using the reconstructed phase currents is within ±0.1 rad, which is promising. By using the proposed scheme, the cost of IPMSM drive system can be significantly reduced and the

reliability can be improved accordingly.

REFERENCES

[1] Z. Wang, Y. B. Wang, J. Chen, and M. Cheng, " Fault tolerant control of NPC three-level inverters fed double-stator-winding PMSM drives based on vector space decomposition," *IEEE Trans. Ind. Electron.,* DOI: 10.1109/TIE.2017.2701782, 2017.

[2] Z. Y. Zeng, W. Y. Zheng, and R. X. Zhao, "Performance Analysis of the Zero-Voltage Vector Distribution in Three-Phase Four-Switch Converter Using a Space Vector Approach," *IEEE Trans. Power Electron.,* vol. 32, no. 1, pp. 260-273, Jan., 2017.

[3] D. H. Zhou, J. Zhao, and Y. Liu, "Predictive Torque Control Scheme for Three-Phase Four-Switch Inverter-Fed Induction Motor Drives With DC-Link Voltages Offset Suppression," *IEEE Trans. Power Electron.,* vol. 30, no. 6, pp. 3309-3318, June, 2015.

[4] M. S. Diab, A. Elserougi, A. M. Massoud, A. S. A. Khalik, and S. Ahmed, "A Four-Switch Three-Phase SEPIC-Based Inverter," *IEEE Trans. Power Electron.,* vol. 30, no. 9, pp. 4891-4905, Sep., 2015.

[5] N. M. A. Freire and A. J. M. Cardoso, "A Fault-Tolerant PMSG Drive for Wind Turbine Applications With Minimal Increase of the Hardware Requirements," *IEEE Trans. Ind. Appl.,* vol. 50, no. 3, pp. 2039-2049, May/June, 2014.

[6] N. M. A. Freire and A. J. M. Cardoso, "A Fault-Tolerant Direct Controlled PMSG Drive for Wind Energy Conversion Systems," *IEEE Trans. Ind. Electron.,* vol. 61, no. 2, pp. 821-834, Feb., 2014.

[7] C. L. Xia, Y. W. Xiao, T. N. Shi, and W. Chen, "Boost Three-Effective-Vector Current Control Scheme for a Brushless DC Motor With Novel Five-Switch Three-Phase Topology," *IEEE Trans. Power Electron.,* vol. 29, no. 12, pp. 6581-6592, Dec., 2014.

[8] B. E. Badsi, B. Bouzidi, and A. Masmoudi, "DTC Scheme for a Four-Switch Inverter-Fed Induction Motor Emulating the Six-Switch Inverter Operation," *IEEE Trans. Power Electron.,* vol. 28, no. 7, pp. 3528-3538, July, 2013.

[9] S. Dasgupta, S. N. Mohan, S. K. Sahoo, and S. K. Panda, "Application of Four-Switch-Based Three-Phase Grid-Connected Inverter to Connect Renewable Energy Source to a Generalized Unbalanced Microgrid System," *IEEE Trans. Ind. Electron.,* vol. 60, no. 3, pp. 1204-1215, Mar., 2013.

[10] R. Wang, J. Zhao, and Y. Liu, "A Comprehensive Investigation of Four-Switch Three-Phase Voltage Source Inverter Based on Double Fourier Integral Analysis," *IEEE Trans. Power Electron.,* vol. 26, no. 10, pp. 2774-2787, Oct., 2011.

[11] K. D. Hoang, Z. Q. Zhu, and M. P. Foster, "Influence and Compensation of Inverter Voltage Drop in Direct Torque-Controlled Four-Switch Three-Phase PM Brushless AC Drives," *IEEE Trans. Power Electron.,* vol. 26, no. 8, pp. 2343-2357, Aug., 2011.

[12] C. L. Xia, Z. Q. Li, and T. N. Shi, "A Control Strategy for Four-Switch Three-Phase Brushless DC Motor Using Single Current Sensor," *IEEE Trans. Ind. Electron.,* vol. 56, no. 6, pp. 2058-2066, June, 2009.

[13] M. N. Uddin, T. S. Radwan, and M. A. Rahman, "Fuzzy-logic-controller-based cost-effective four-switch three-phase inverter-fed IPM synchronous motor drive system," *IEEE Trans. Ind. Appl.,* vol. 42, no. 1, pp. 21-30, Jan./Feb., 2006.

[14] M. B. D. R. Corrêa, C. B. Jacobina, E. R. C. D. Silva, and A. M. N. Lima, "A General PWM Strategy for Four-Switch Three-Phase Inverters," *IEEE Trans. Power Electron.,* vol. 21, no. 6, pp. 1618-1627, Nov., 2006.

[15] B. K. Lee, T. H. Tim, and M. Ehsani, "On the feasibility of four-switch three-phase BLDC motor drives for low cost commercial applications: topology and control," *IEEE Trans. Power Electron.,* vol. 18, no. 1, pp. 164-172, Jan., 2003.

[16] F. Blaabjerg, D. A. Neacsu, and John K. Pedersen, "Adaptive SVM to Compensate DC-Link Voltage Ripple for Four-Switch Three-Phase Voltage-Source Inverters," *IEEE Trans. Power Electron.,* vol. 14, no. 4, pp. 743-752, July, 1999.

[17] A. Gaeta, G. Scelba, and A. Consoli, "Sensorless Vector Control of PM Synchronous Motors During Single-Phase Open-Circuit Faulted Conditions," *IEEE Trans. Ind. Appl.,* vol. 48, no. 6, pp. 1968-1979, Nov./Dec., 2012.

[18] S. Medjmadj, D. Diallo, M. Mostefai, C. Delpha, and A. Arias, "PMSM Drive Position Estimation: Contribution to the High-Frequency Injection Voltage Selection Issue," *IEEE Trans. Energy Convers.,* vol. 30, no. 1, pp. 349-358, Mar., 2015.

[19] B. Akin, U. Orguner, A. Ersak, and M. Ehsani, "Simple Derivative-Free Nonlinear State Observer for Sensorless AC Drives," *IEEE/ASME Trans. Mechatronics,* vol. 11, no. 5, pp. 634-643, Oct., 2006.

[20] P. L. Xu and Z. Q. Zhu, "Novel Square-Wave Signal Injection Method Using Zero-Sequence Voltage for Sensorless Control of PMSM Drives," *IEEE Trans. Ind. Electron.,* vol. 63, no. 12, pp. 7444-7454, Dec., 2016.

[21] S. B. Ozturk and H. A. Toliyat, "Direct Torque and Indirect Flux Control of Brushless DC Motor," *IEEE/ASME Trans. Mechatronics,* vol. 16, no. 2, pp. 351-360, Mar., 2010.

[22] T. D. Nguyen, G. Foo, K. J. Tseng and D. M. Vilathgamuwa, "Modeling and Sensorless Direct Torque and Flux Control of a Dual-Airgap Axial Flux Permanent-Magnet Machine With Field-Weakening Operation," *IEEE/ASME Trans. Mechatronics,* vol. 19, no. 2, pp. 412-422, Apr., 2014.

[23] G. L. Wang, L. Yang, G. Q. Zhang, X. G. Zhang, and D. G. Xu, "Comparative Investigation of Pseudorandom High-Frequency Signal Injection Schemes for Sensorless IPMSM Drives," *IEEE Trans. Power Electron.,* vol. 32, no. 3, pp. 2123-2132, Mar., 2017.

[24] X. D. Sun, L. Chen, Z. B. Yang and H. Q. Zhu, "Speed-Sensorless Vector Control of a Bearingless Induction Motor With Artificial Neural Network Inverse Speed Observer," *IEEE/ASME Trans. Mechatronics,* vol. 18, no. 4, pp. 1357-1366, Aug., 2013.

[25] A. H. Niasar, A. Vahedi, and H. Moghbelli, "A Novel Position Sensorless Control of a Four-Switch, Brushless DC Motor Drive Without Phase Shifter," *IEEE Trans. Power Electron.,* vol. 23, no. 6, pp. 3079-3087, Nov., 2008.

[26] C. T. Lin, C. W. Hung, and C. W. Liu, "Position Sensorless Control for Four-Switch Three-Phase Brushless DC Motor Drives," *IEEE Trans. Power Electron.,* vol. 23, no. 1, pp. 438-444, Jan., 2008.

[27] Y. Y. Li and G. T. C. Chiu, "Control of loudspeakers using disturbance-observer-type velocity estimation," *IEEE/ASME Trans. Mechatronics,* vol. 10, no. 1, pp. 111-117, Feb., 2005.

[28] Z. Wang, Y. Zheng, Z. X. Zou, and M. Cheng, "Position sensorless control of interleaved CSI fed PMSM drive with extended Kalman filter," *IEEE Trans. Magn.,* vol. 48, no. 11, pp. 3688-3691, Nov. 2012.

[29] Y. X. Xu, H. Yan, J. B. Zou, B. C. Wang, and Y. H. Li, "Zero Voltage Vector Sampling Method for PMSM Three-Phase Current Reconstruction Using Single Current Sensor," *IEEE Trans. Power Electron.,* vol. 32, no. 5, pp. 3797-3807, May, 2017.

[30] H. F. Lu, X. M. Cheng, W. L. Qu, S. Sheng, Y. T. Li, and Z. Y. Wang, "A Three-Phase Current Reconstruction Technique Using Single DC Current Sensor Based on TSPWM," *IEEE Trans. Power Electron.,* vol. 29, no. 3, pp. 1542-1550, Mar., 2014.

[31] B. Hafez, A. S. A. Khalik, A. M. Massoud, S. Ahmed, and R. D. Lorenz, "Single-Sensor-Based Three-Phase Permanent-Magnet Synchronous Motor Drive System With Luenberger Observers for Motor Line Current Reconstruction," *IEEE Trans. Ind. Appl.,* vol. 50, no. 4, pp. 2602-2613, July/Aug., 2014.

[32] Y. S. Lai, Y. K. Lin, and C. W. Chen, "New Hybrid Pulsewidth Modulation Technique to Reduce Current Distortion and Extend Current Reconstruction Range for a Three-Phase Inverter Using Only DC-link Sensor," *IEEE Trans. Power Electron.,* vol. 28, no. 3, pp. 1331-1337, Mar., 2013.

[33] Y. Cho, T. LaBella, and J. S. Lai, "A Three-Phase Current Reconstruction Strategy With Online Current Offset Compensation Using a Single Current Sensor," *IEEE Trans. Ind. Electron.,* vol. 59, no. 7, pp. 2924-2933, July, 2012.

[34] Y. K. Gu, F. L. Ni, D. P. Yang, and H. Liu, "Switching-State Phase Shift Method for Three-Phase-Current Reconstruction With a Single DC-Link Current Sensor," *IEEE Trans. Ind. Electron.,* vol. 58, no. 11, pp. 5186-5194, Nov., 2011.

[35] K. Sun, Q. Wei, L. P. Huang, and K. Matsuse, "An Overmodulation Method for PWM-Inverter-Fed IPMSM Drive With Single Current Sensor," *IEEE Trans. Ind. Electron.,* vol. 57, no. 10, pp. 3395-3404, Oct., 2010.

[36] J. I. Ha, "Voltage Injection Method for Three-Phase Current Reconstruction in PWM Inverters Using a Single Sensor," *IEEE Trans. Power Electron.,* vol. 24, no. 3, pp. 767-775, Mar., 2009.

[37] D. P. Marčetić and E. M. Adžić, "Improved Three-Phase Current Reconstruction for Induction Motor Drives With DC-Link Shunt," *IEEE Trans. Ind. Electron.,* vol. 57, no. 7, pp. 2454-2462, July, 2010.

[38] H. Kim and T. M. Jahns, "Phase Current Reconstruction for AC Motor Drives Using a DC Link Single Current Sensor and Measurement Voltage Vectors," *IEEE Trans. Power Electron.,* vol. 21, no. 5, pp. 1413-1419, Sep., 2006.

[39] W. C. Lee, D. S. Hyun, and T. K. Lee, "A Novel Control Method for Three-Phase PWM Rectifiers Using a Single Current Sensor," *IEEE Trans. Power Electron.,* vol. 15, no. 5, pp. 861-870, Sep., 2000.